Applied Catalysis B: Environmental 182 (2016) 236–246

Contents lists available at ScienceDirect

Applied Catalysis B: Environmental

journal homepage: www.elsevier.com/locate/apcatb

Aqueous phase electrocatalysis and thermal catalysis for the hydrogenation of phenol at mild conditions

Yang Song[a], Oliver Y. Gutiérrez[a,*], Juan Herranz[b], Johannes A. Lercher[a,*]

[a] TU München, Department of Chemistry and Catalysis Research Center, Lichtenbergstrasse 4, D-84747 Garching, Germany
[b] TU München, Chair of Technical Electrochemistry, Lichtenbergstrasse 4, D-85748 Garching, Germany

ARTICLE INFO

Article history:
Received 1 July 2015
Received in revised form 7 September 2015
Accepted 12 September 2015
Available online 14 September 2015

Keywords:
Electrocatalysis
Aromatic hydrogenation
Noble metal catalysts
Biomass conversion

ABSTRACT

The electrocatalytic hydrogenation (ECH) of phenol on Pt/C, Rh/C, and Pd/C was explored in an H-type two-compartment cell with respect to the impact of electrolyte, pH, current, and catalyst concentration. In all cases, the electric efficiencies increased with increasing phenol conversions. Rh/C exhibited the highest hydrogenation rate normalized to the concentration of accessible metal (TOF) followed by Pt/C in terms of mass of metal and intrinsic activities. Therefore, the effect of temperature on ECH and of mild thermal hydrogenation (TH) of phenol was explored on these catalysts. The activation energies for ECH were ca. 23 kJ/mol and 29 kJ/mol on Rh/C, and Pt/C, respectively. TH is much faster than ECH, although both pathways have the same activation energy. Cyclic voltammetry of bulk Pt and Pt/C in the presence of phenol indicated that phenol is adsorbed on the metal and reacted with hydrogen radicals. Hence, ECH was concluded to proceed *via* a Langmuir-type mechanism where the surface hydrogen is produced by reduction of protons (which occurs when the catalyst contacts the electrode) instead of H_2 dissociation as in TH. Although competitive reactions evolve H_2 during ECH, the involvement of this H_2 in phenol hydrogenation was minor. Thus, ECH and TH are independent processes and do not exhibit any synergy. In both pathways, the reaction path is phenol → cyclohexanone → cyclohexanol. C—O bond cleavage was not observed.

1. Introduction

Reductive biomass conversion and electricity generation from renewable sources (e.g., photovoltaics, wind power, and hydropower) are essential to secure a sustainable supply of energy, fuels, and chemicals [1–4]. Most of the techniques that are emerging for producing biofuels from biomass-derived feedstocks require H_2 to remove oxygen from the biogenic material [5–7]. Whereas, H_2 may not be available in the decentralized locations, excess electricity generated from renewable resources may be stored supplying the reduction equivalents. Thus, coupling electrochemical water reduction with the reduction of biomass-derived feedstocks would help to improve the utilization of wind and solar energy by storing energy *via* reduction of the locally available feedstock.

The electrocatalytic hydrogenation (ECH) of biomass is beginning to emerge as a conceptually attractive alternative for thermal upgrading bio-oil at mild conditions using reduction equivalents generated by electricity [8,9]. During ECH, $H^{\bullet}$ is formed on the surface of the catalyst *via* reduction of protons supplied by the electrolyte, hydrogenating organic substrates. The conversions are ideally achieved at mild conditions and the overpotential required for ECH can be minimized by adapting the electrocatalyst [10].

Lignocellulosic biomass deconstructed *via* thermal or chemical methods is easily available at a local level, stimulating substantial efforts in the catalytic reduction of complex mixtures to fuels and chemicals [11,12]. Exploring the conversion of compounds, representative of deconstructed biomass, on well-defined materials is critical to elucidate structure-activity correlations needed for the development of better catalysts, which must be stable in the presence of substantial concentrations of water associated with the treatment of bio-oils [13]. Estimulating efforts on the conversion of representative compounds in aqueous phase have been reported in literature [14,15]. However, classical electrochemical mechanisms have been given for granted and the involvement of thermal pathways is a question that is not addressed. Conversion routes accessed by thermal catalysis might be relevant at mild conditions over metals that offer the highest activity and stability in electrochemical processes performed in aqueous solutions. Comparing thermal catalysis and electrocatalysis is of prime importance as H_2

* Corresponding authors. Fax: +49 89 28913544.
E-mail addresses: Oliver.Gutierrez@mytum.de (O.Y. Gutiérrez), Johannes.Lercher@ch.tum.de (J.A. Lercher).

http://dx.doi.org/10.1016/j.apcatb.2015.09.027
0926-3373/

produced from water electrolysis can be used as external H_2 supply to maximize hydrogenation efficiency.

Thus, the present work investigates the performance of a series of C-supported noble metal catalysts (Pt, Pd, and Rh) integrated in an electrolytic cell for the cathodic transformation of phenol in aqueous phase. The effects of electrolyte, current, pH and temperature on selectivity, intrinsic activity (TOF) and electrical efficiency of the catalysts are described. ECH is compared with thermal catalysis at the same mild conditions in order to understand the reaction mechanisms.

2. Experimental

2.1. Chemicals and catalytic materials

All chemicals were obtained from Sigma–Aldrich and used as received, i.e., phenol (≥99.0%), acetate buffer solution (pH 4.6), phosphoric acid (≥99.9%), acetic acid (≥99.0%), sulfuric acid (≥99.9%), toluene (≥99.9%, HPLC), ethyl acetate (≥99.9%, HPLC), NaOH (≥99.9%, HPLC), and KCl (≥99.0%). High purity water, obtained with a Milli-Q water purification system with a resistivity of 18.2 MΩ cm, was used for all experiments. The supported noble metal catalysts used in this study were purchased from Sigma–Aldrich: Pt/C, Pd/C, and Rh/C. All these materials had a metal content of 5 wt.%.

2.2. Catalyst characterization

The surface areas and pore diameters of the catalysts were determined by N_2 adsorption at 77 K on a PMI automated BET sorptometer. The samples were outgassed before measurements at 523 K for 20 h. The surface areas and pore distributions were calculated according to BET and BJH models.

The dispersion of the metal phase was determined by H_2 chemisorption. Prior to the measurements, the materials were treated under vacuum at 588 K for 1 h and then cooled to 313 K. Hydrogen adsorption isotherms were measured at 1–40 kPa H_2. After equilibration with H_2, the samples were outgassed at 313 K for 1 h and a second set of isotherms was measured. The concentrations of chemisorbed H_2 on the metal were determined by extrapolating the difference isotherms to zero hydrogen pressure. The dispersion of the supported metals was estimated from the concentration of chemisorbed H_2 assuming a stoichiometry of 1:1 metal to hydrogen atoms.

The dispersion of the metal was also explored by transmission electron microscopy (TEM). Samples of the catalysts were ground, and ultrasonically dispersed in ethanol. Drops of the suspensions were applied on a copper–carbon grid and the measurements were carried out in a JEOL JEM-2011 electron microscope with an accelerating voltage of 120 keV. Statistical treatment of the metal particle size was done by counting at least 200 particles detected in several places of the grid.

2.3. Electrocatalytic hydrogenation (ECH)

Electrolysis was carried out at atmospheric pressure in an H-type two-compartment electrochemical cell with a jacket for temperature control. Typically, the temperature was kept at 296 K (room temperature), except during a series of experiments performed at temperatures up to 353 K. The two compartments of the cell were separated by a Nafion 117 proton exchange membrane (Ion Power, Inc.), which was treated in sulfuric acid (2 M) before use. A piece of reticulated vitreous carbon (RVC, ERG Aerospace Corp., 100 pores per inch) shaped into a 20 mm × 20 mm × 12 mm cuboid, and connected to a graphite rod (Sigma–Aldrich), was used as working electrode in the cathode compartment. A Pt wire (Alfa Aesar, 99.9%) was used as counter electrode in the anode compartment. The reference electrode was a home-made Ag/AgCl electrode with a double junction. The cathode compartment was filled with 58 mL of electrolyte solutions at defined pH (adjusted by adding small amounts of aqueous NaOH or the corresponding acid). A chosen amount of catalyst was added into liquid at the cathode compartment as powder, stirring the slurry at 500 rpm. Prior to ECH, polarization of the catalyst was performed under a constant current of −40 mA for 30 min. After polarization, 2 mL of phenol solution was added into the cathode compartment to obtain a final concentration of 17.7 mmol/L. ECH was then performed at galvanostatic (−40 mA) or potentiostatic (−0.72 V on Pt/C and −0.65 V on Rh/C) conditions, while a flow of N_2 was maintained through the cell. During all these described procedures, the anode compartment was filled with 40 mL of solution containing the corresponding electrolyte. All electrochemical procedures were performed with an electrochemical workstation (VSP-300, Bio Logic). Before each ECH test (and before the voltammetric experiments described below), the cell compartments and other materials were cleaned with concentrated H_2SO_4 and immersed in boiling water for 2 h several times. Prior to the reactions, the electrodes were alternatively immersed in H_2SO_4 (5 M) and KOH (5 M) for 15 min. After each immersion, the materials were thoroughly cleaned (Pt electrodes were further ultrasonically treated) in ultrapure water for 15 min.

2.4. Catalytic hydrogenation (CH) and additional electrochemical measurements

Catalytic hydrogenation (i.e., thermal, with and without the presence of any electric potential) was carried out at atmospheric pressure of H_2 at constant temperature. This was achieved by flowing 20 mL/h of H_2 through the solution in the cathode compartment. The concentration of phenol was kept at 17.7 mmol/L, whereas, different amounts of catalyst was used (to control the reaction rates) suspended in the solution and magnetically stirred at constant rate. Electrocatalytic hydrogenation in the presence of H_2 (20 mL/h) was performed following the procedure for the ECH process mentioned above.

Selected cyclic voltammetric experiments were performed using Pt wires as cathode and anode. An Ag/AgCl electrode was used as reference electrode, whereas, the electrolyte was an aqueous solution of acetic acid at pH 5. The potential window from −0.5 V to 0.9 V was applied with a scan rate of 20 mV/s. CVs were performed using a RVC cathode with a potential window from −1.4 V to 0.2 V and a scan rate of 20 mV/s.

2.5. Product analysis

The course of the ECH and CH experiments was followed by periodically withdrawing aliquots of 1 mL from the cathode compartment. The products were extracted with 3 mL of ethyl acetate. The organic phase (ethyl acetate) was separated from the aqueous phase by decantation and dried on Na_2SO_4. 1 mL of the dry organic phase was mixed with 0.5 mL of a solution containing toluene as standard. Quantitative analyses of those samples were performed by gas chromatography coupled with mass spectrometry (Shimadzu GC–MS-QP2010), equipped with a plot Q capillary column (30 m × 250 μm) and a thermal conductivity detector (TCD).

3. Results and discussion

3.1. Physicochemical properties of catalysts

The textural properties of the catalytic materials are compiled in Table 1. All materials exhibit comparably high specific surface areas and pore volumes. Microporosity, also comparable for all materials,

Table 1
Textural properties and metal particle size of carbon-supported metal catalysts.

	BET surface area ($m^2\ g^{-1}$)	Mesopore surface area ($m^2\ g^{-1}$)	Micropore volume ($cm^3\ g^{-1}$)	Total pore volume ($cm^3\ g^{-1}$)
Pt/C	957	301	0.34	0.709
Pd/C	744	233	0.3	0.662
Rh/C	921	288	0.26	0.729

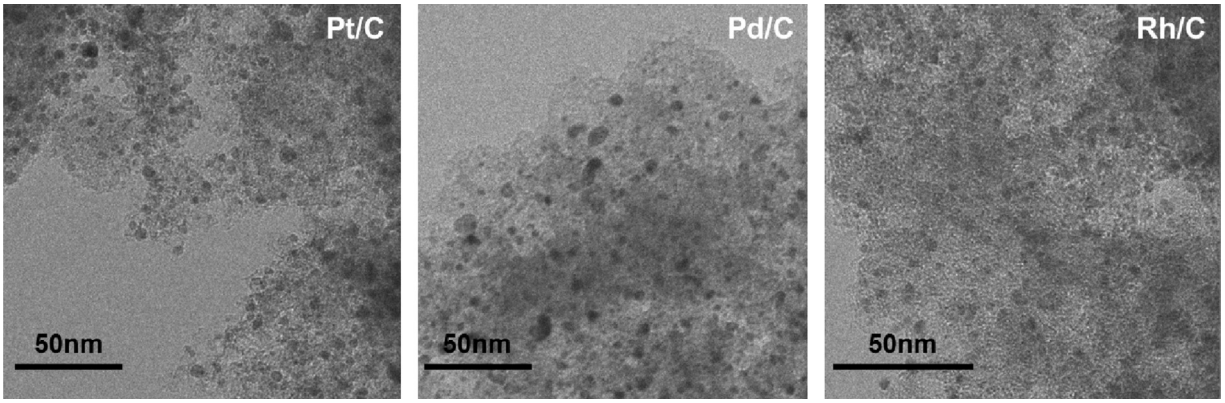

Fig. 1. Representative TEM micrographs of Pt/C, Pd/C, and Rh/C.

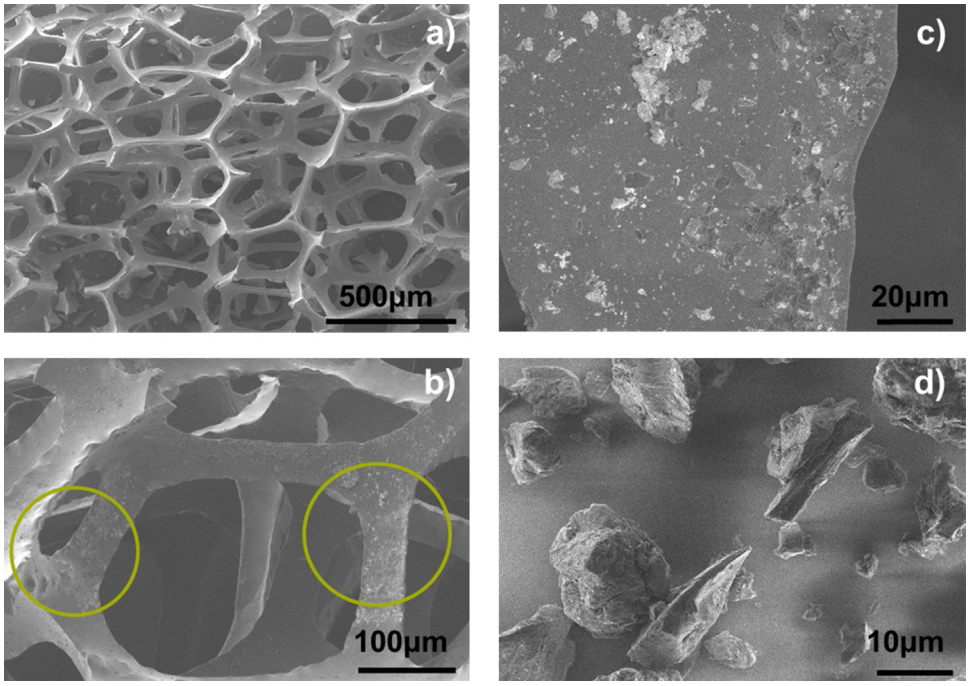

Fig. 2. SEM images of selected materials after ECH reactions: bare RVC (100 ppi) (a); SEM images of RVC covered with Pt/C (b) and (c); SEM image of Pt/C particles (d).

is the major contribution to the overall pore volume. The average particle size, as determined by H_2 chemisorption was 2.7, 2.1, and 3.4 nm, for Pt/C, Pd/C, and Rh/C, respectively. These particle sizes were in reasonable agreement with the sizes estimated from TEM images (Fig. 1). That is 3.3 nm for Pt/C, and Pd/C, and 3.9 nm for Rh/C. The particle sizes determined by TEM are larger than those determined by H_2 likely because some small particles escaped from detection in microscopy.

Reticulated vitreous carbon (RVC) of 100 pores per inch (100 ppi, surface area of 66 cm^2 per cm^3) was selected as working electrode. This material has been widely applied in electrochemistry due to its high surface area, high conductivity, and good mechanical strength [16,17]. The microscopic morphology of RVC was characterized by HR-SEM. Fig. 2 presents the typical carbon network that characterizes the morphology of RVC. The images in the Figure were taken from materials tested in ECH experiments. Therefore, particles of catalyst (Pt/C), of around 1–10 µm, could also be visualized as granular material. Light spots on the granules are identified as domains with abundant concentrations of Pt particles.

3.2. Impact of reaction parameters on the electrocatalytic hydrogenation of phenol

The activities of the catalysts were tested in the electrocatalytic hydrogenation (ECH) of phenol in the presence of three different electrolytes at pH 5 with a current of −40 mA. The amount of

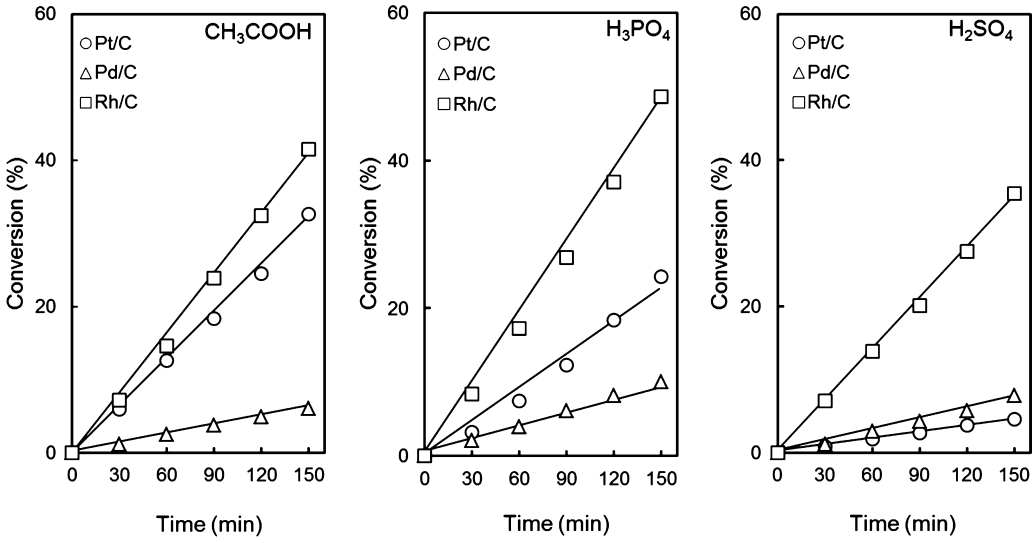

Fig. 3. Conversion of phenol on different catalysts, and in the presence of selected electrolytes. All reactions were performed at −40 mA, room temperature, pH 5, and with 50 mg of catalyst.

Table 2
ECH rate (mol/s g_{metal}), TOF (h^{-1}), and EE (%) under different electrolyte and catalyst.

	Acetic acid			Phosphoric acid			Sulfuric acid		
	Rate[a]	TOF[b]	EE[c]	Rate	TOFs	EE	Rate	TOF	EE
Pt/C	1.5×10^{-5}	28.8	41	1.1×10^{-5}	19.7	30.5	3.5×10^{-6}	6.7	5.8
Pd/C	2.9×10^{-6}	6.5	7.6	4.1×10^{-6}	7.4	12.5	2.2×10^{-6}	3.9	10
Rh/C	1.8×10^{-5}	33.7	52.2	2.1×10^{-5}	38.7	66.5	1.6×10^{-5}	30.2	58.8

[a] reaction rate calculated as shown in the supporting information.
[b] turn over frequency calculated with the dispersion obtained by H_2 chemisorption.
[c] electrical efficiency calculated as shown in the supporting information.

catalysts, added as slurry to the cathode compartment with the RVC electrode, was 50 mg in all experiments. As shown in Fig. 3, the trend in activity of the catalysts did hardly depend on the electrolyte. Namely, Rh/C was the most active material followed by Pt/C, whereas, Pd/C showed very low activities.

The use of acetic acid as electrolyte leads to the highest activities for Rh/C and Pt/C, followed by phosphoric acid, whereas, the use of sulfuric acid leads to the lowest conversions. The beneficial effect of acetic acid on the hydrogenation of phenol over alumina-supported Pd catalysts has been attributed to the adsorption of the acid on the support, which eases the adsorption of phenol *via* electrostatic forces [18–20]. However, on the catalysts explored, acetic acid reduced the rate of phenol hydrogenation, likely due to competitive adsorption on the metal surface. Therefore, we hypothesize that phosphate and sulfate ions adsorb on the metal surface stronger than acetic acid, which leads to lower rates in the presence of the former two electrolytes. The performance of Pd/C, poor compared to Rh/C and Pt/C, was not affected by the nature of the electrolyte to a significant extent.

ECH rates, turnover frequencies (TOFs) and electrical efficiencies (EE) calculated from the experiments reported in Fig. 3 are shown in Table 2. As expected, the ECH rates follow the same trends described for phenol conversion. Rh/C converts 1.6×10^{-5} – 2.1×10^{-5} mol of phenol per second and gram of metal, Pt/C slightly less than that, i.e., 1.1×10^{-5}–1.5×10^{-5} mol/s g_{metal} (in the presence of sulfuric acid, the ECH rate on Pt/C decreases by one order of magnitude). The conversion rates on Pd/C are in the range of 2.2×10^{-6} – 4.1×10^{-6} mol/s g_{metal}. In terms of TOF, the differences are more evident, Rh/C is an outstanding catalyst with TOF values from 30 to 38 h^{-1}. In comparison, the intrinsic activity of Pt/C depends stronger on the electrolyte exhibiting TOFs from 6.7 to 28 h^{-1}. The intrinsic activity of Pd/C was also low, i.e., in the range of 4–6.5 h^{-1}. Interestingly, the electrical efficiency (EE) of the catalysts (the percentage of electrons used to hydrogenate phenol, see the supporting information), is proportional to the conversion rates of phenol. That is, Rh/C leads to the highest EE (between 50% and 66%), followed by Pt/C (between 5.8% and 41%). Evidently, Pt/C and Rh/C are the most active catalysts and acetic acid is a suitable electrolyte to perform the reaction on both catalysts. Therefore, the following experiments focus on ECH of phenol on Pt/C and Rh/C in the presence of acetic acid.

ECH of phenol was performed on Pt/C and Rh/C under galvanostatic conditions at −20 mA, −40 mA and −60 mA. The conversion of phenol is shown in Fig. 4. The higher the current input, the higher the conversion of phenol. This is not surprising as increasing the input of electrons should accelerate the conversion of phenol (at least as long as the phenol concentration at the metal surface is not the limiting reactant). At all conditions, the conversion of phenol on Rh/C is faster than on Pt/C, e.g., 3.5×10^{-5} mol/s g_{metal} on Rh/C, compared to 2.6×10^{-5} mol/s g_{metal} on Pt/C at −60 mA. Note that the increase in phenol conversion is not linearly proportional to the current increase. Varying the current from −20 mA to −40 mA, and −60 mA, which corresponds to current increases by two and three, respectively, leads to increases of ECH rates and TOFs of nearly 7 and 13 times (Table 3). This is attributed to the low potentials generated at −20 mA, which are −0.55 V (vs Ag/AgCl) on Pt/C and −0.53 V (vs Ag/AgCl) on Rh/C. These potentials are close to the theoretical potential of hydrogen evolution reaction (HER) of −0.523 V as calculated for the conditions of the experiments (the calculation is shown in the supporting information). In contrast, at −40 mA, and −60 mA, the potentials generated are < −0.65 V, and < −0.75 V, respectively. This leads to higher overpotentials to drive the ECH.

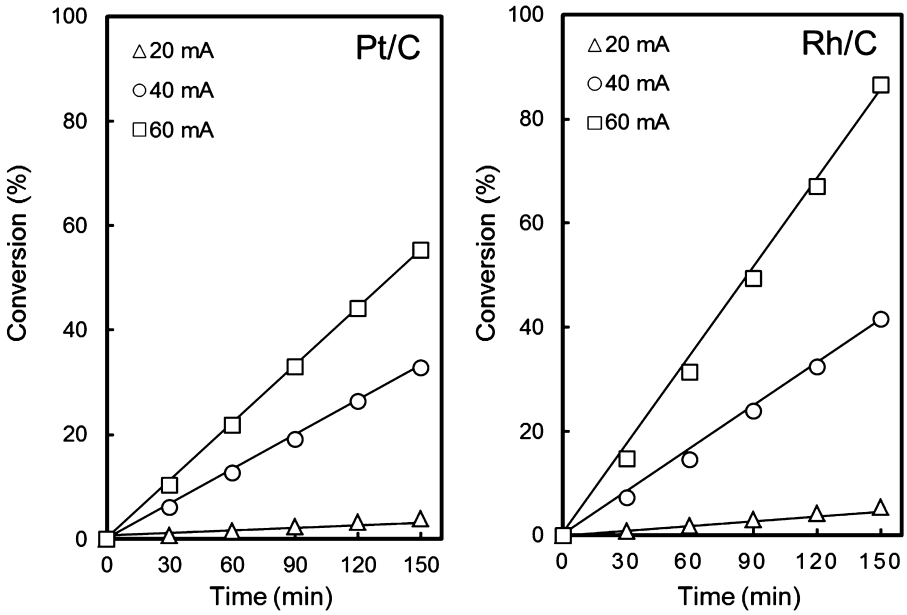

Fig. 4. Conversion of phenol under different currents on Pt/C (left) and Rh/C (right). The reactions were performed at room temperature, pH 5, in acetic acid, with 50 mg of catalyst.

Table 3
Potential, reaction rate (mol/s g_{metal}), TOF (h^{-1}), and EE (%), observed in the ECH of phenol on Pt/C and Rh/C under several conditions.

		Pt/C				Rh/C			
		Potential[a]	Rate[b]	TOF[c]	EE[d]	Potential[a]	Rate[b]	TOF[c]	EE[d]
Current Input[e], mA	−20	−0.55	1.8×10^{-6}	3.4	9.6	−0.53	2.5×10^{-6}	4.6	13
	−40	−0.68	1.5×10^{-5}	28.8	40	−0.65	1.8×10^{-5}	34	52
	−60	−0.96	2.6×10^{-5}	46.8	45	−0.71	3.5×10^{-5}	66	77
Catalyst amount[f], mg	20	−0.73	1.1×10^{-5}	20.5	11	−0.67	3.9×10^{-5}	74	44
	50	−0.68	1.5×10^{-5}	28.8	40	−0.65	1.8×10^{-5}	34	52
	200	−0.67	3.7×10^{-6}	6.8	39	−0.64	4.4×10^{-6}	8	54
Solution pH[g]	3	−0.61	1.3×10^{-5}	23.4	29	−0.57	1.6×10^{-5}	29	44
	5	−0.68	1.5×10^{-5}	28.8	40	−0.65	1.8×10^{-5}	34	52
	10	−1.25	8.2×10^{-6}	15.5	24	−1.05	2.5×10^{-5}	46	95

[a] potential E with respect to Ag/AgCl (V).
[b] reaction rate calculated as shown in the supporting information.
[c] turn over frequency calculated with the dispersion obtained by H_2 chemisorption.
[d] electrical efficiency calculated as shown in the supporting information.
[e] 50 mg of catalyst and pH of 5.
[f] −40 mA and pH of 5.
[g] 50 mg of catalyst and −40 mA.

Varying amounts of catalysts (20 mg, 50 mg and 200 mg) were used in ECH of phenol on Pt/C and Rh/C. The observed dependences of conversion on time and amount of catalysts are shown in Fig. 5. The use of 50 mg leads to substantial increases of phenol conversion, compared to using only 20 mg. However, increasing the amount of catalyst to 200 mg does not increase the conversion rates further. This implies that, under the experimental conditions, the rate of electron transfer does not vary when stirring 50 mg or 200 mg of powder catalyst.

It is reported that the pH of the solution plays an important role on the conversion rates of biomass-derived compounds conversions *via* ECH [21–24]. ECH of phenol with Pt/C and Rh/C at initial pH values of 3, 5, and 10 was carried out in the presence of acetic acid. The catalytic performance is reported in Fig. 6. Interestingly, the dependences on pH are different on both catalysts. The conversion rate on Pt/C is 1.3×10^{-5} mol/s g_{metal} at pH 3, 1.5×10^{-5} mol/s g_{metal} at pH 5, and decreases to 8.2×10^{-6} mol/s g_{metal} at pH 10. In contrast, the conversion rate on Rh/C increases with increasing pH, i.e., 1.6×10^{-5} mol/s g_{metal} at pH 3, 1.8×10^{-5} mol/s g_{metal} at pH 5, and 2.5×10^{-5} mol/s g_{metal} at pH 10. There is not a straightforward explanation for these different trends. The complication arises from the fact that the distribution of species in solution changes dramatically in the range of pH explored. Besides the decreasing concentration of protons in solutions with increasing pH, acetic acid (electrolyte) and phenol are present in neutral forms at pH 3. At pH 5 acetic acid ($pK_a = 4.75$) is present as acetate, whereas at pH 10, phenol ($pK_a = 9.95$) produces phenolate anions. The concentration of chemical species on the surface of the solids has to be influenced by those changes in solution, and it may also be affected by the charge of the solid surface at different pH values (point of zero charge of the carbon). We hypothesize that the factor determining the rates of ECH at varying pH is the adsorption of phenol on the metal particles as the slowest ECH rates are observed at pH 3 (the condition with the highest concentration of protons in solution among the explored conditions). Further analysis will be addressed in ongoing studies.

Table 3 summarizes the rates, TOF, and EE values determined for the ECH of phenol on Pt/C, and Rh/C under varying currents,

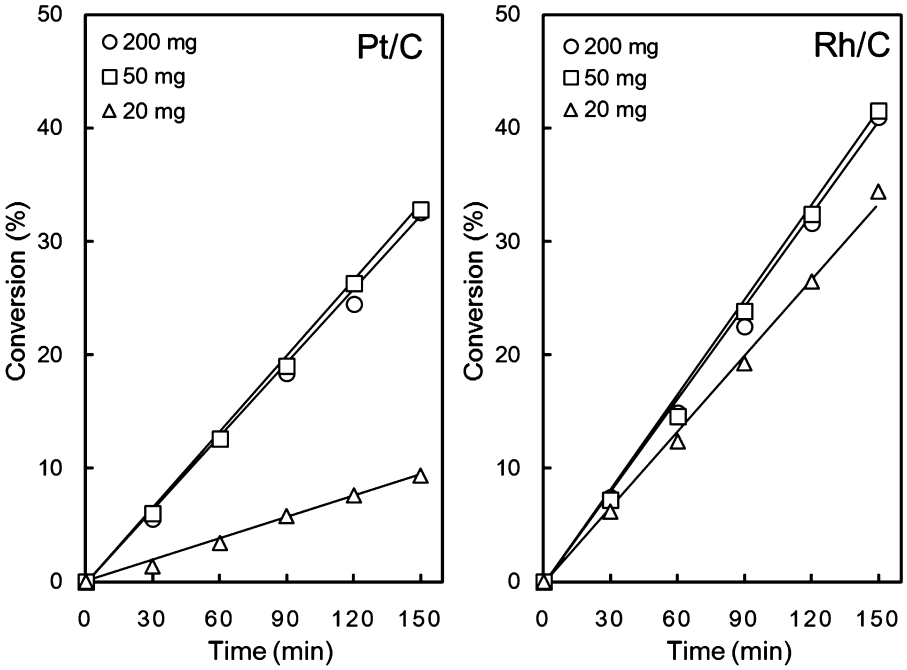

Fig. 5. Conversion of phenol with varying amount of catalyst, Pt/C (left) and Rh/C (right). The reactions were performed at room temperature, −40 mA, pH 5, in acetic acid.

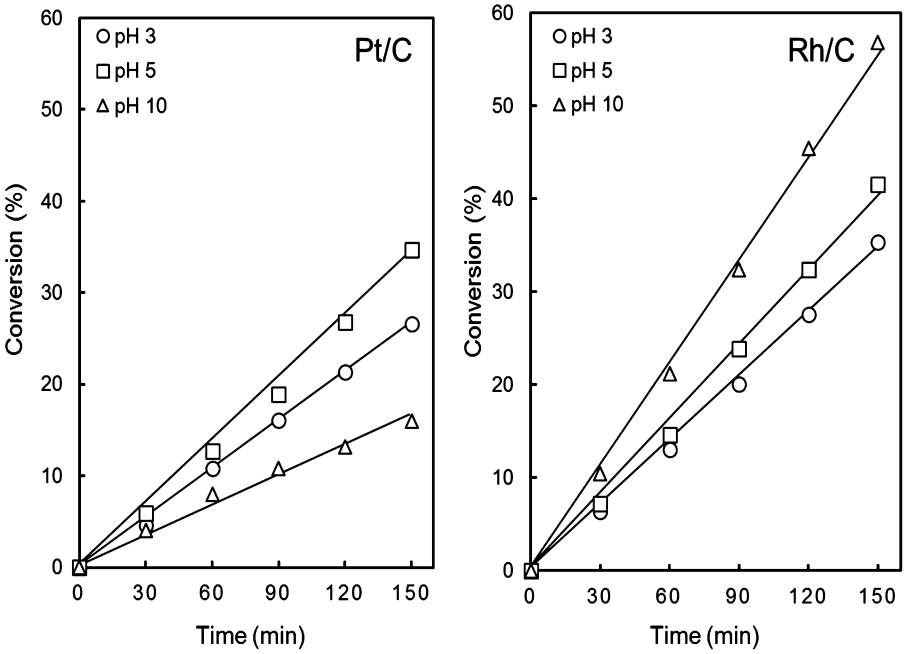

Fig. 6. Conversion of phenol in solutions of acetic acid at varying pH on Pt/C (right) and Rh/C (left).

amount of catalyst and pH. Under all conditions, Rh/C exhibited higher weight specific (per gram of catalyst) and intrinsic activity (TOF) than Pt/C. Interestingly, the higher the activities (conversion rates and TOF), the higher the associated electric efficiencies. This is very relevant as it implies that improving the performance of the catalyst would also improve the energy utilization associated to the process. We would like to highlight the fact that the potentials observed at pH 10 were −1.25 V and −1.05 V, for Pt/C and Rh/C, respectively (last entry in Table 3). This is significantly more negative than the potentials observed at lower pH values. It suggests that the identity of the hydrocarbon species being hydrogenated on the metal changes by increasing the pH to 10. Furthermore, the activity of Pt is severely affected by the change reflected with this potential as its activity for ECH drops at pH 10. Another outstanding result is the extremely high EE (95%) obtained on Rh/C at pH 10. This high efficiency reflects the fact that phenol was almost quantitatively converted to cyclohexanol, which consumes 6 electrons per molecule of phenol converted.

3.3. Impact of temperature on the ECH and thermal hydrogenation of phenol

The effect of temperature on the ECH of phenol was studied under galvanostatic and potentiostatic conditions with acetic acid

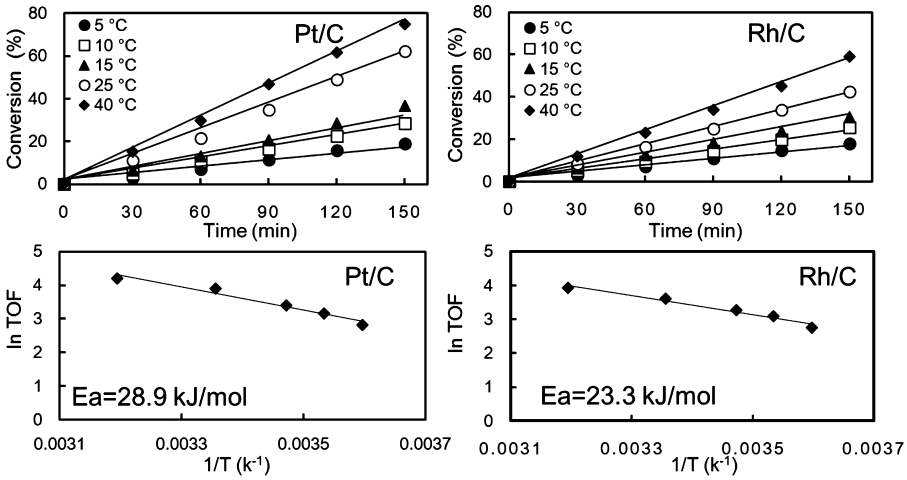

Fig. 7. Conversion of phenol along with time at varying temperatures on Pt/C and Rh/C (upper panels). Arrhenius plots for the ECH of phenol on Pt/C (−0.75 V vs Ag/AgCl) and Rh/C (−0.62 V vs Ag/AgCl) (lower panels). The reactions were performed with 50 mg Pt/C or 20 mg Rh/C in acetic acid at pH 5.

as electrolyte (pH 5). In a preliminary study, the phenol ECH was explored on Pt/C in the temperature range of 5–80 °C with −40 mA. The conversion increased with temperature up to 50 °C. However, at 50 °C or above, the catalyst quickly deactivated. These results are shown in the supporting information (Fig. S1). Deactivation of the catalyst has also been observed in Refs. [25,26]. The activation energy, calculated from the conversion rates of phenol below 50 °C, was 7 kJ/mol. This unusual value is attributed to the reaction rate being limited by the supply of electrons due to the use of galvanostatic conditions (the proton reduction cannot be faster than the current input).

At potentiostatic conditions, the dependence of phenol conversion on temperature was determined on Pt/C and Rh/C from 5 °C to 40 °C as shown in Fig. 7. The corresponding activation energies, calculated using TOF values were 29 kJ/mol on Pt/C, and 23 kJ/mol on Rh/C (the Arrhenius plots are presented in Fig. 7).

In order to understand the contributions of thermal pathways and the ECH mechanism, thermal hydrogenation (TH) of phenol was carried out on Pt/C. Namely, bubbling H_2 through the solution containing phenol, acetic acid, and the catalyst (Pt/C) in the absence of electric potential. The variation of conversion with temperature and time, and the Arrhenius plot are presented in Fig. 8. The apparent energy of activation corresponding to the TH of phenol at mild conditions was 33 kJ/mol, which is in good agreement with the values reported for TH at high temperatures [27–29]. More importantly, this activation energy is very similar to that found for the ECH of phenol (29 kJ/mol, vide supra). This indicates that ECH and TH of phenol have the same rate-determining step (the mechanistic implications are further discussed below). Rates, TOFs and EEs of the experiments performed at varying temperatures are summarized in Table 4. As previously noted, the EE increased with the rate of phenol conversion. Therefore, within the studied range, EE increases with increasing temperature.

For comparison, the TH of phenol was performed at room temperature in pure water. The conversion rate of phenol was higher (7.6×10^{-5} mol/s g_{metal}) in pure water than in the presence of acetic acid (6.4×10^{-5} mol/s g_{metal}). The concentration profiles are presented in Fig. S2 of the supporting information. This implies that acetic acid (needed as electrolyte for ECH) slows down the hydrogenation likely due to competitive adsorption on the metal.

3.4. Study of the reaction network and mechanism

In all the experiments reported in this work, the only products of the reaction were cyclohexanone and cylohexanol. Typical profiles

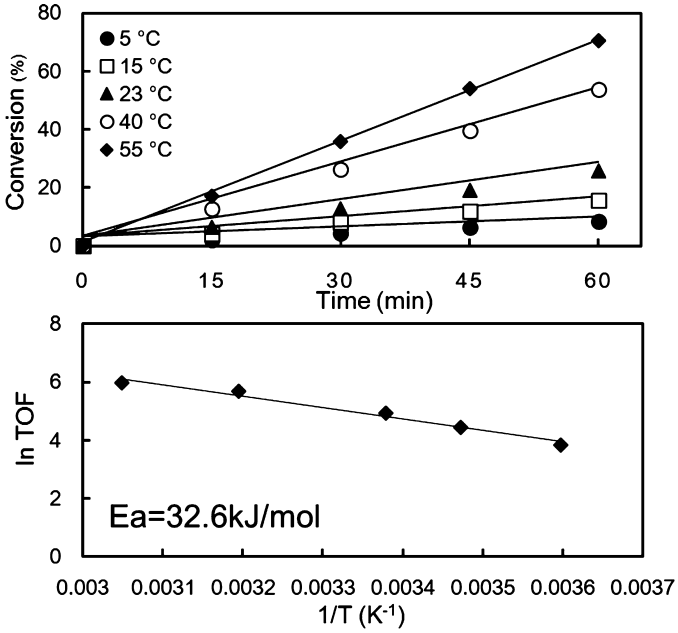

Fig. 8. Conversion of phenol during thermal conversion along with time at varying temperatures on Pt/C (upper panels), and the corresponding Arrhenius plot (lower panels). The reactions were performed at atmospheric pressure, 20 mg of catalyst in acetic acid at pH 5.

of the concentrations of reactant and products are shown in Fig. 9. As expected from the nature of the products, cyclohexanone is the primary product observed as well as an intermediate (the concentration of cyclohexanone increases with time and decreases after reaching a maximum), whereas cyclohexanol is a secondary and stable product (the concentration of cyclohexanol increases exponentially with time up to an inflection point, which corresponds to the maximum in cyclohexanone concentration). Cleavage of the C—O bond is not observed under any reaction conditions applied in this study. Thus, phenol is hydrogenated to cyclohexanone, which is in turn hydrogenated to cyclohexanol. The two steps need four and two atoms of hydrogen, respectively, which are provided by the reduction of protons from the solution (Scheme 1).

The ECH of phenol was carried out on Pt/C (50 mg of catalyst with acetic acid as electrolyte at pH 5) using three different experimental configurations in order to clarify the macroscopic mechanism of the reaction. The “suspension” configuration has been described in

Table 4
Reaction rate (mol/s g_{metal}), TOF (h^{-1}), and EE (%), observed for the ECH of phenol at varying temperatures.

	Pt/C			Rh/C		
Temperature	Rate	TOF	E.E	Rate	TOF	EE
5 °C	9×10^{-6}	16.6	26.4	8.5×10^{-6}	15.8	35
10 °C	1.3×10^{-5}	23.5	36.1	1.2×10^{-5}	21.9	44.8
15 °C	1.6×10^{-5}	30.2	41.8	1.4×10^{-5}	26.3	47.6
25 °C	2.7×10^{-5}	49.5	55.4	2×10^{-5}	37.1	54.1
40 °C	3.6×10^{-5}	67.4	62.1	2.7×10^{-5}	50.6	63.1

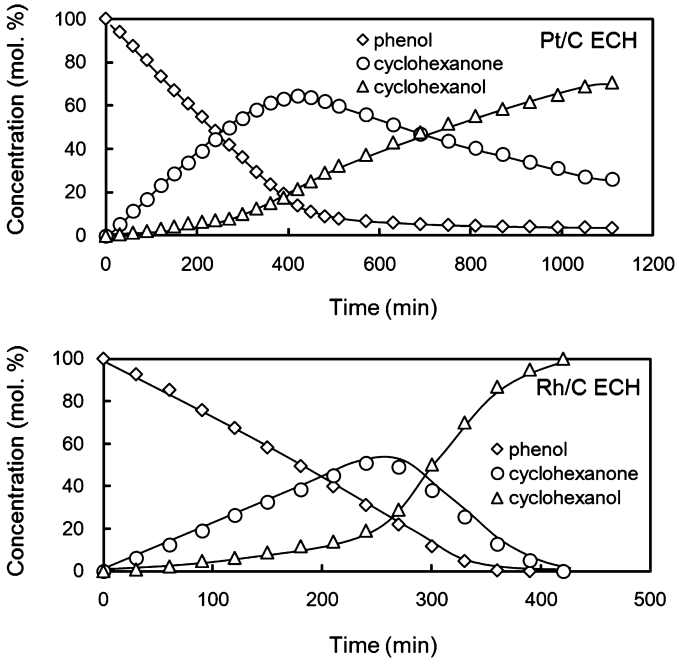

Fig. 9. Concentration profiles of phenol and the products of ECH (cyclohexanone, and cyclohexanol) on Pt/C and Rh/C. The experiments were performed at −40 mA, room temperature, in acetic acid with pH 5.

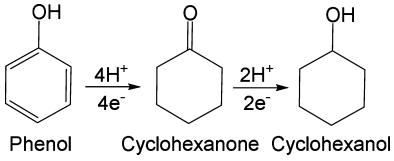

Scheme 1. Reaction network for the electrocatalytic hydrogenation of phenol on Pt/C, and Rh/C.

detail in the experimental part and consisted in suspending the catalyst in the reactant solution containing the working electrode (RVC electrode) and performing the reaction with stirring. The "filter" configuration consisted in introducing the catalyst inside a porous container into the reactant solution in order to avoid direct contact of the powder with the electrode. In the "ink" configuration, an ink containing the catalyst was prepared according to Ref. [30]. This ink was applied onto the RVC electrode in order to deposit the desired amount of catalyst directly on it. Fig. S3 shows the phenol conversions observed with these three configurations. Table S1 summarizes the reaction rates, TOF and EE values. The "filter" configuration led to negligible phenol conversion, demonstrating that the direct contact between the catalyst grains and the electrode was needed to perform the reaction (the ECH process does not involved molecular charged species). Another implication of this experiment was that the concentration of H_2 in solution (generated at the cathode during the experiment), was insufficient to hydrogenate phenol to a significant extent *via* thermal pathways (vide infra). The

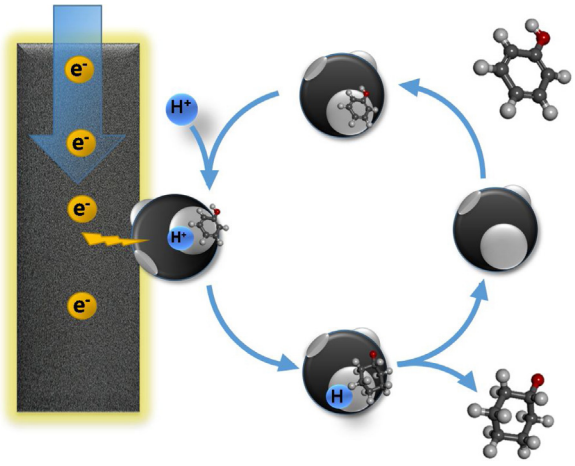

Fig. 10. Visualization of the macroscopic process for the electrocatalytic hydrogenation of phenol with a carbon-supported metal catalyst is suspension.

"ink" configuration led to about half of the phenol conversion rate with respect to the "suspension" configuration (although the same amount of catalyst was present in both kind of experiments), i.e., 1.5×10^{-5} mol/s g_{Pt} ("suspension") and 6×10^{-6} mol/s g_{Pt} ("ink"). This observation was unexpected as a constant and direct contact between the metal and the electrode should have ensured a continuous flow of electrons for the ECH (which may be not the case for the "suspension" configuration). We attribute this observation to possible agglomeration of the catalyst particles during the preparation and deposition of the ink, and covering of the metal particles with the polymers needed to prepare the ink. These could have easily reduced the proportion of metal accessible during the reaction.

Hence, the macroscopic ECH process during "suspension" operation is concluded to occur as shown in Fig. 10. Phenol molecules and protons adsorb on the metal supported on carbon particles suspended in solution. The particles of the catalyst contact the electrode, which allows the transfer of electrons, which reduce the protons on the metal particles. Finally, there is a surface reaction between hydrogen radicals and adsorbed phenol producing the hydrogenated product, which desorbs.

In order to gain understanding on the microscopic mechanism of ECH, cyclic voltammetry (CV) studies were performed on bulk Pt and the Pt/C catalyst interacting with phenol. Cyclic voltammetry was performed on a Pt wire as cathode at pH 5 and a potential window between 1 V and −0.8 V vs Ag/AgCl. As shown in Fig. 11a, the typical curve of a Pt electrode was observed in pure electrolyte solution. The maxima in cathodic and anodic current correspond to the Reactions (1)–(4), where *-H^+ and *-H denote protons and hydrogen atoms adsorbed on metal sites, respectively. That is, hydrogen oxidation and oxide formation in the anodic part, and metal reduction and hydrogen evolution in the cathodic part [31,32].

$$^* + H^+ + e^- \rightleftharpoons {}^*\text{-H}\quad \text{Reversible hydrogen underpotential deposition} \tag{1}$$

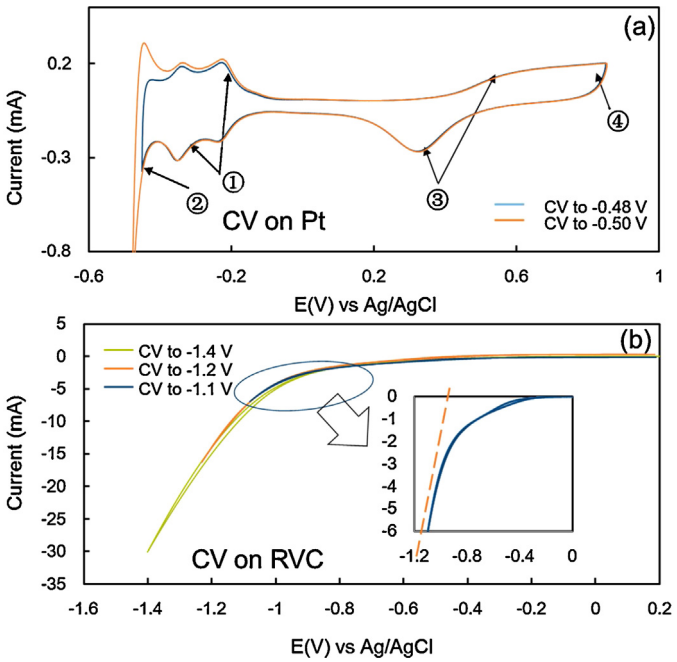

Fig. 11. Cyclic voltamogramms on the Pt cathode at varying overpotential, (a). Cyclic voltamogramms on RVC cathode at varying overpotential, (b). CVs are performed in acetic acid with pH 5, at a scan rate of 20 mV/s.

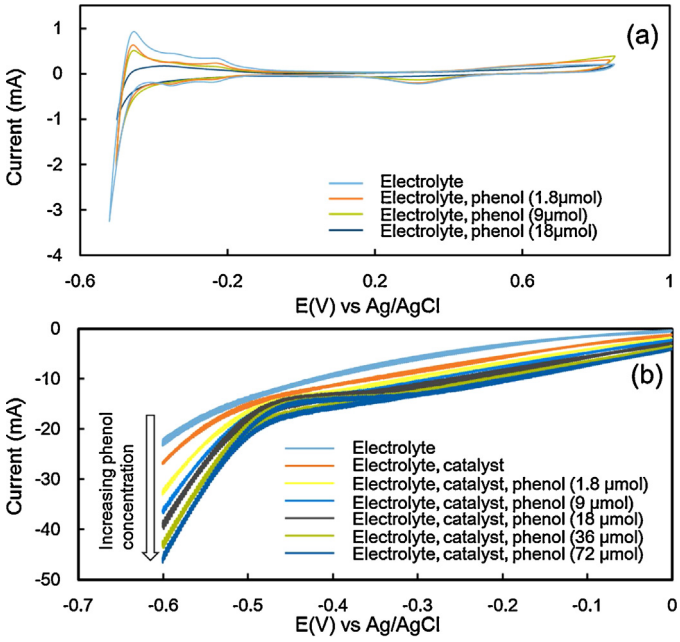

Fig. 12. Cyclic voltagramms on the Pt cathode at varying concentration of phenol, (a). Cyclic voltagramms on the RVC cathode with Pt/C as catalyst, at different concentration of phenol. CVs are performed in acetic acid with pH 5, at a scan rate of 20 mV/s.

$$2H^+ + 2e^- \rightarrow H_2\uparrow \text{ Hydrogen evolution reaction} \quad (2)$$

$$Pt + 2OH^- \rightleftharpoons Pt\text{–}O + H_2O + 2e^- \text{ Reversible Pt hydroxide/oxide formation} \quad (3)$$

$$H_2O \rightarrow \tfrac{1}{2}O_2\uparrow + 2H^+ + 2e^- \text{ Oxygen evolution reaction} \quad (4)$$

The potential of the H_2 evolution reaction (HER) shown in the voltagramm of Fig. 11(a), at about −0.52 V (vs Ag/AgCl), is in good agreement with the value predicted by the Nernst equation. Fig. 12a shows the CV curves in the presence of increasing concentrations of phenol. Evidently, all current maxima fade out in the presence of phenol, i.e., the reacting substrate hinders all the surface reactions by adsorbing strongly on the metal surface.

The CV of the bare RVC electrode was also studied in the range of 0.2 V and −1.6 V as shown in Fig. 11b. HER was observed at potentials more negative than −1.1 V (vs Ag/AgCl), much more negative to the one on bare Pt wire or in the presence of Pt/C (vide infra). Current peaks for the reversible hydrogen reduction–oxidation were not observed on bare RVC. Fig. 12a and b show the CV curves obtained with an RVC electrode in the presence of Pt/C and increasing concentrations of phenol. The increase of cathodic current is observed at around −0.52 V, confirming that the transformations described along this work was driven by the proton reduction occurring on the Pt particles of the Pt/C powder in contact with the electrode. More interestingly, increasing concentrations of phenol lead to currents that are more negative. This indicates that the presence of phenol accelerates the reduction of protons. Note that the addition of phenol did not change the pH noticeably. In turn, we attribute this observation to the reduction of hydrocarbon species on the metal surface, which scavenges hydrogen atoms allowing faster adsorption and reduction of protons.

Thus, the microscopic mechanism of phenol hydrogenation under ECH can be described with the series of Reactions (5)–(10), where the symbol "*-" denotes an adsorbed species, and "*" is an unoccupied metal site. C_nH_{2n-6}, and C_nH_{2n-4} denote an aromatic species and the corresponding hydrogenated product, respectively. Adsorbed hydrogen and molecular hydrogen are produced *via* Volmer, Herovsky, and Tafel reactions (5)–(7) [33–35]. The hydrocarbon, on the other hand, adsorbs on the metal sites (8), and then undergoes hydrogenation with hydrogen radicals. Reaction (9) illustrates a one-step hydrogenation process for the sake of simplicity. However, the hydrogenation of adsorbed hydrocarbons is most likely stepwise. Finally, a stable hydrogenated species desorbs to give the product of the reaction (10). Clearly, the hydrogenation of adsorbed hydrocarbons and H_2 evolution (Heyrovsky and Tafel reactions) are parallel and competing reactions. Furthermore, the increasing EE values with increasing temperature (ECH experiments reported in Table 4), indicate that the rate of hydrocarbon hydrogenation increases faster than that of hydrogen evolution.

$$H^+ + e^- + {}^* \rightarrow {}^*\text{-H Volmer reaction} \quad (5)$$

$$^*\text{-H} + H^+ + e^- \rightarrow H_2 \text{ Heyrovsky reaction} \quad (6)$$

$$2\,^*\text{-H} \rightleftharpoons H_2 \text{ Tafel reaction} \quad (7)$$

$$^* + C_nH_{2n-6} \rightleftharpoons {}^*\text{-}C_nH_{2n-6} \quad (8)$$

$$2\,^*\text{-H} + {}^*\text{-}C_nH_{2n-6} \rightarrow {}^*\text{-}C_nH_{2n-4} + {}^* \quad (9)$$

$$^*\text{-}C_nH_{2n-4} \rightleftharpoons C_nH_{2n-4} + {}^* \quad (10)$$

3.5. Comparison of ECH and TH of phenol

The thermal hydrogenation (TH) of phenol (in the absence of electric potential) follows a Langmuir–Hinshelwood mechanism. H_2 adsorbs on the metal dissociatively to form adsorbed hydrogen atoms, according to Reaction (11):

$$H_2 + 2^* \rightleftharpoons 2\,^*\text{-H} \quad (11)$$

The adsorption, subsequent hydrogenation of the hydrocarbon and evolution of the product proceed as described by Reactions (8)–(10). Therefore, ECH and TH of phenol differ only in the origin

Table 5
Reaction rates (mol/s g_{metal}), and TOFs (h^{-1}), observed for the hydrogenation of phenol on Pt/C and Rh/C during different experimental conditions. ECH: electrocatalytic hydrogenation; TH: thermal hydrogenation; ECH + TH: ECH and TH performed simultaneously.

Reaction path	Pt/C		Rh/C	
	Rate	TOFs	rate	TOFs
ECH[a]	1.5×10^{-5}	28. 8	3.96×10^{-5}	73.5
TH[b]	6.4×10^{-5}	118.8	2.05×10^{-4}	380.7
ECH+TH[c]	8×10^{-5}	151.2	2.44×10^{-4}	452.8

[a] ECH was performed at −40 mA, and room temperature, in acetic acid (pH 5). 50 mg of Pt/C or 20 mg of Rh/C were used.
[b] TH was performed in acetic acid (pH 5) with H_2 at atmospheric pressure and room temperature. 50 mg of Pt/C or 20 mg of Rh/C were used.
[c] ECH + TH was performed at −40 mA, and room temperature, in acetic acid (pH 5) in the presence of flowing H_2 at atmospheric pressure. 50 mg of Pt/C or 20 mg of Rh/C were used.

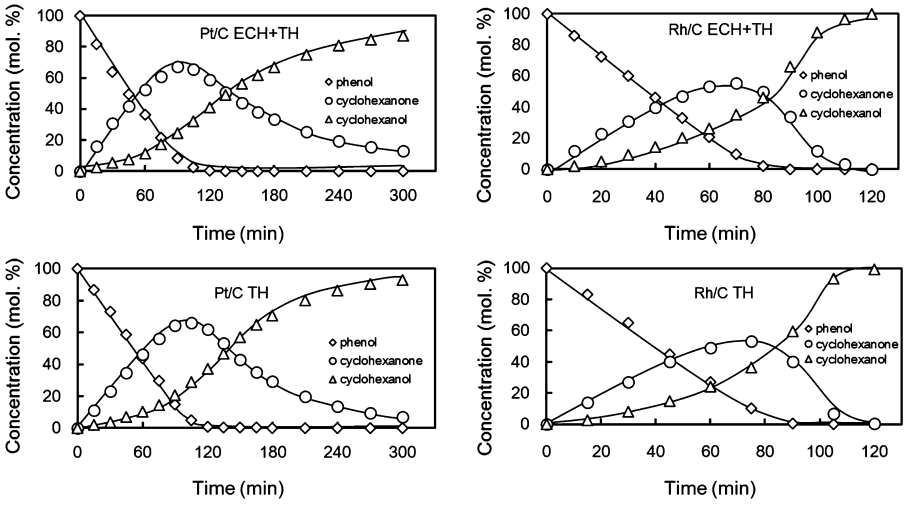

Fig. 13. Concentration profiles of phenol and the products on Pt/C during thermal hydrogenation (TH) (a), and simultaneous TH and electrocatalytic hydrogenation (ECH + TH) (b). Concentration profiles of phenol and the products on Rt/C during TH (c), and ECH + TH (d). The ECH + TH experiments were performed at −40 mA, room temperature, in acetic acid (pH 5) under H_2 flow (atmospheric pressure). 50 mg Pt/C and 20 mg Rh/C are chosen amount of catalyst. The TH experiments were performed at the same conditions in the absence of any electric potential.

of the adsorbed hydrogen species. The identical activation energies of ECH and TH on Pt/C, suggests that both processes have the same rate determining step, i.e., one of the hydrogenation steps included in Reaction (9) [36,37].

ECH and TH were compared by performing the hydrogenation of phenol on Pt/C and Rh/C under ECH, or TH conditions only, and ECH-TH, namely, ECH in the presence of H_2 (or thermal hydrogenation in the presence of the electric potential). The results of phenol ECH under typical galvanostatic reaction conditions (−40 mA in acetic acid at pH 5) are summarized in Table 5 (concentration profiles are shown in Fig. 13). The concentration profiles observed during TH are shown in Fig. 13, whereas the rates of phenol conversion and TOFs on Pt/C and Rh/C are compiled in Table 5. Obviously, TH of phenol is much faster than phenol ECH, i.e., 4 and 5 times on Pt/C and Rh/C, respectively. The phenol conversion rates and TOFs obtained during the ECH-TH experiments are shown in Table 5, whereas the concentration profiles are shown in Fig. 13. Remarkably, the rates and TOFs of the catalysts in the ECH-TH experiments equal the sum of the values observed during ECH and TH. This observation has several important implications, i.e., TH and ECH are independent pathways (hydrogen radicals for ECH are those produced from proton reduction instead of re-adsorbed H_2), and there is no synergy between electric potential and thermally catalyzed pathways.

Discussing concentration profiles observed on Pt/C and Rh/C highlights the similarities and differences of their intrinsic catalytic properties. On both catalysts, the decrease of phenol concentration is linear up to almost full conversion indicating that the reaction is zero order with respect to phenol. Furthermore, the concentration of cyclohexanone peaks at almost full conversion of phenol on both catalysts. This indicates that the rates of phenol hydrogenation are significantly faster than those of cyclohexanone hydrogenation, although the former step needs four H (consuming four electrons), whereas, cyclohexanone hydrogenation consumes only two H (two electrons). Rh/C is 2–3 times more active than Pt/C. Furthermore, the concentration of cyclohexanone peaks at shorter reaction time on Rh/C than on Pt/C. Also the hydrogenation of cyclohexanone was faster on Rh/C than on Pt/C, as the ratios of initial production rates cyclohexanone/cyclohexanol were ca. 5.2 and 3.9, respectively. The final product was cyclohexanol in all cases, e.g., C—O bond cleavage was not observed. It is speculated that the activation energy for hydrogenolysis is much higher than for hydrogenation. Therefore, it requires much higher temperatures and/or overpotentials than those accessed in this study.

4. Conclusions

This work explores the conversion of phenol on Pt/C, Rh/C, and Pd/C (5 wt.% metal) *via* electrocatalysis (electrocatalytic hydrogenation, ECH) and mild thermal catalysis (TH). The results show that ECH of phenol can be realized using suspensions of catalysts in the presence of a reticulated vitreous carbon electrode. Varying the electrolyte, the highest rates were found with acetic acid at pH 5.

In the temperature range studied (5 °C–50 °C), TH and ECH have the same activation energy (~30 kJ/mol on Pt/C), which guides us to the conclusion that both pathways have the identical rate determining step. The electrocatalytic hydrogenation of phenol occurs *via* a Langmuir–Hinshelwood mechanism in which H^+ and the sub-

strate are adsorbed on the catalyst metal particles. The protons are reduced upon contact of the catalyst with the electrode, which produces adsorbed hydrogen radicals that hydrogenate the adsorbed hydrocarbons. Recombination of $H^{\bullet}$ occurs in parallel (H_2 evolution reaction) competing with hydrogenation. Compared to the ECH pathway, TH (where adsorbed H is produced by dissociation of H_2) is faster, likely due to much higher H coverage. The two pathways (ECH and TH) are independent, i.e., in the presence of the electrochemical reduction the evolved H_2 does not contribute in a measurable way to the overall reaction. In both pathways, the reaction network is phenol → cyclohexanone → cyclohexanol. C—O bond cleavage is not observed, in line with thermal catalysis in the absence of acid sites enabling deoxygenation *via* acid catalyzed dehydration. Electrocatalytic hydrogenation can be achieved under conditions similar to thermal conversions. The efficiency of the reaction depends markedly on the adsorption of the hydrocarbon on the metal and on the possibility to eliminate H_2 evolution.

Acknowledgement

The authors would like to thank Prof. Hubert A. Gasteiger and his group at the Technische Universität München for fruitful discussions. We are also grateful to Dr. Erika Ember for experimental and scientific advice, Dr. Marianne Hanzlik for TEM measurements, and to Dipl.-Ing. Xaver Hecht for technical support.

Appendix A. Supplementary data

Supplementary data associated with this article can be found, in the online version, at http://dx.doi.org/10.1016/j.apcatb.2015.09.027.

References

[1] S.J. Davis, K. Caldeira, H.D. Matthews, Science 329 (2010) 1330–1333.
[2] A.J. Ragauskas, C.K. Williams, B.H. Davison, G. Britovsek, J. Cairney, C.A. Eckert, W.J. Frederick, J.P. Hallett, D.J. Leak, C.L. Liotta, J.R. Mielenz, R. Murphy, R. Templer, T. Tschaplinski, Science 311 (2006) 484–489.
[3] A. Corma, S. Iborra, A. Velty, Chem. Rev. 107 (2007) 2411–2502.
[4] K. Christopher, R. Dimitrios, Energy Environ. Sci. 5 (2012) 6640–6651.
[5] C. Zhao, J. He, A.A. Lemonidou, X. Li, J.A. Lercher, J. Catal. 280 (2011) 8–16.
[6] S. Czernik, A.V. Bridgwater, Energy Fuels 18 (2004) 590–598.
[7] C. Zhao, Y. Kou, A.A. Lemonidou, X. Li, J.A. Lercher, Angew. Chem. Int. Ed. 48 (2009) 4047–4050.
[8] D. Robin, M. Comtois, A. Martel, R. Lemieux, A.K. Cheong, G. Belot, J. Lessard, Can. J. Chem. 68 (1990) 1218–1227.
[9] Z. Li, M. Garedew, C.H. Lam, J.E. Jackson, D.J. Miller, C.M. Saffron, Green Chem. 14 (2012) 2540–2549.
[10] X. Han, F. Cheng, T. Zhang, J. Yang, J. Hu, J. Chen, Adv. Mater. 26 (2014) 2047–2051.
[11] A.J. Ragauskas, G.T. Beckham, M.J. Biddy, R. Chandra, F. Chen, M.F. Davis, C.E. Wyman, Science 344 (2014) 1246843-1–1246843-10.
[12] C. Li, M. Zheng, A. Wang, T. Zhang, Energy Environ. Sci. 5 (2012) 6383–6390.
[13] X. Xu, Y. Li, Y. Gong, P. Zhang, H. Li, Y. Wang, J. Am. Chem. Soc. 134 (2012) 16987–16990.
[14] F. Laplante, L. Brossard, H. Ménard, Can. J. Chem. 81 (2003) 258–264.
[15] C.M. Cirtiu, A. Brisach-Wittmeyer, H. Ménard, J. Catal. 245 (2007) 191–197.
[16] J.M. Friedrich, C. Ponce-de-León, G.W. Reade, F.C. Walsh, J. Electroanal. Chem. 561 (2004) 203–217.
[17] J. Wang, Electrochim. Acta 26 (1981) 1721–1726.
[18] A. Martel, B. Mahdavi, J. Lessard, H. Ménard, L. Brossard, Can. J. Chem. 75 (1997) 1862–1867.
[19] P.S. Guin, S. Das, P.C. Mandal, Int. J. Electrochem. 2011 (2011) 1–22.
[20] C.M. Cirtiu, H.O. Hassani, N.A. Bouchard, P.A. Rowntree, H. Ménard, Langmuir 22 (2006) 6414–6421.
[21] M.A. Casadei, D. Pletcher, Electrochim. Acta 33 (1988) 117–120.
[22] D.S. Santana, G.O. Melo, M.V.F. Lima, J.R. Daniel, M.C. Areias, M. Navarro, J. Electroanal. Chem. 569 (2004) 71–78.
[23] M.A. Casadei, D. Pletcher, Electrochim. Acta 33 (1988) 117–120.
[24] Y. Mao, B.M. Fung, J. Colloid Interface Sci. 191 (1997) 216–221.
[25] B. Zhao, M. Chen, Q. Guo, Y. Fu, Electrochim. Acta 135 (2014) 139–146.
[26] S.K. Green, J. Lee, H.J. Kim, G.A. Tompsett, W.B. Kim, G.W. Huber, Green Chem. 15 (2013) 1869–1879.
[27] J. He, C. Zhao, J.A. Lercher, J. Catal. 309 (2014) 362–375.
[28] J. He, C. Zhao, D. Mei, J.A. Lercher, J. Catal. 309 (2014) 280–290.
[29] F. Colmati, E. Antolini, E.R. Gonzalez, J. Power Sources 157 (2006) 98–103.
[30] T.J. Schmidt, H.A. Gasteiger, G.D. Stäb, P.M. Urban, D.M. Kolb, R.J. Behm, J. Electrochem. Soc. 145 (1998) 2354–2358.
[31] M.H. Miles, M.A. Thomason, J. Electrochem. Soc. 123 (1976) 1459–1461.
[32] S.A. Grigoriev, M.S. Mamat, K.A. Dzhus, G.S. Walker, P. Millet, Int. J. Hydrogen Energy 36 (2011) 4143–4147.
[33] Y. Kwon, M. Koper, ChemSusChem 6 (2013) 455–462.
[34] A. Bannari, P. Proulx, H. Ménard, C.M. Cirtiu, Appl. Catal. A: Gen. 345 (2008) 28–42.
[35] P.J. Rheinländer, J. Herranz, J. Durst, H.A. Gasteiger, J. Electrochem. Soc. 161 (2014) F1448–F1457.
[36] V.R. Stamenkovic, B.S. Mun, M. Arenz, K.J. Mayrhofer, C.A. Lucas, G. Wang, N.M. Markovic, Nat. Mater. 6 (2007) 241–247.
[37] M. Besson, P. Gallezot, C. Pinel, Chem. Rev. 114 (2013) 1827–1870.